Effect of Hydrodynamic Forces on Virus Removal Capability of Planova™ Filters

Aguru Yamamoto
Analysis and Simulation Center, Asahi Kasei Corporation, Fuji-shi, Shizuoka 416-8501, Japan

Tomoko Hongo-Hirasaki
Bioprocess Technology Development Dept., Asahi Kasei Medical MT Co., Ltd., 5-4960 Nakagawara-machi, Nobeoka-shi, Miyazaki 882-0031, Japan

Yukihiko Uchi
Analysis and Simulation Center, Asahi Kasei Corporation, Fuji-shi, Shizuoka 416-8501, Japan

Hirohisa Hayashida and Fujiharu Nagoya
Bioprocess Technology Development Dept., Asahi Kasei Medical MT Co., Ltd., 5-4960 Nakagawara-machi, Nobeoka-shi, Miyazaki 882-0031, Japan

DOI 10.1002/aic.14392
Published online February 18, 2014 in Wiley Online Library (wileyonlinelibrary.com)

Virus removal processes are extremely important to biological product safety. This study gives a detailed description of the virus removal mechanisms of Planova™ filters. These include the following: (1) Mechanism 1: size exclusion, (2) Mechanism 2: constraint by hydrodynamic forces, and (3) Mechanism 3: multistep filtration. The process was studied through the dynamic perspective of virus movement using simulations and experiments. Our results show that Mechanism 2 and Brownian motion are key factors in virus removal of size exclusion-based filtration and can be evaluated by Peclet number. The addition of dynamic perspective makes it possible to describe macroscopic phenomena such as the effects of filtration pressure and solution viscosity on virus removal capabilities. © 2014 American Institute of Chemical Engineers *AIChE J*, 60: 2286–2297, 2014

Keywords: hydrodynamic force, Peclet number, nanoparticle, membrane separations, size exclusion

Introduction

Virus removal processes must use advanced separation technologies to remove the minute quantities of viruses existing in protein solutions at highly efficient removal rates. Filtration using virus removal filters is a method that is widely applied in the manufacturing processes of biotherapeutic products. Virus removal filters are composed of separation membranes that capture viruses while allowing proteins to pass through. To secure full confidence in the viral safety of drug products, effective virus removal clearance must be demonstrated and virus removal mechanisms must be fully understood. There are two types of virus removal membranes composing virus removal filters, to remove viruses with thick functional layers[1,2] and with extremely thin layers.[3–5] We studied the virus removal membrane with thick functional layers composing Planova™ filters (hereafter referred to as "Planova filter").

We propose a schematization for the mechanism active in the virus removal in Planova filters according to the following three mechanisms:

1. Size exclusion,
2. Constraint by hydrodynamic forces (Figure 1), and
3. Multistep filtration.

Mechanism 1 is a static factor related to the sizes of viruses and pores. Tsurumi et al.[6] studied the relationship between pore structures and removal mechanisms using a prototype for Planova filters as a model membrane. Tsurumi et al.[7] also investigated localized virus removal mechanisms through experiments using monodisperse gold particles as model particles. The membrane is a porous medium with a pore structure consisting of voids and capillaries. The voids and capillaries are connected like a neural network; the voids correspond to the neurons and the capillaries correspond to the synapses. When $d_{cap} < d_{virus}$, where d_{cap} is the diameter of the capillary and d_{virus} is the diameter of the virus, the virus cannot pass from the void to the capillary and is excluded at the capillary's entrance (Mechanism 1). Because proteins are smaller than viruses, they can pass through the small capillaries and move farther downstream. In this way, the separation of viruses and proteins is accomplished. When $d_{cap} \geq d_{virus}$, the virus passes through from the void into the capillary. However, Planova filters have a succession of voids and capillaries. A virus which happens to be able to pass through one capillary will encounter other waiting voids and capillaries and will have recurring opportunities to be excluded. This continuum of successive size exclusion

Correspondence concerning this article should be addressed to A. Yamamoto at yamamoto.at@om.asahi-kasei.co.jp.

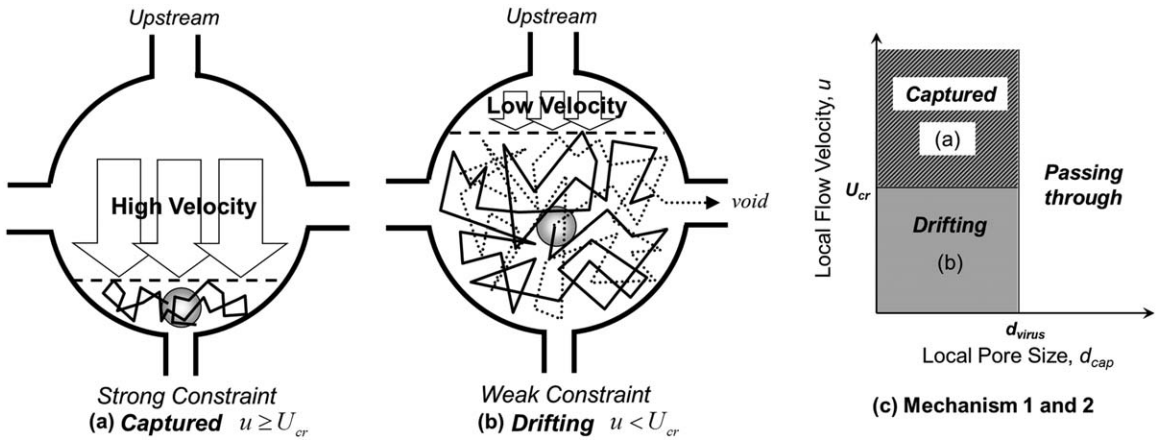

Figure 1. Virus behavior at a capillary entrance.

Here, *u* is the average flow velocity in the downstream capillary and *U*cr is the critical velocity. In (a) and (b), the capillary at the downstream side (i.e., the south side) of the void is smaller than the viruses and the three other capillaries are larger than the viruses. (a) Captured: viruses can be strongly constrained when flow velocity is high. The condition is illustrated in the upper left-hand region of (c). (b) Drifting: viruses are only weakly constrained and their ranges of motion are widened when the flow velocity is low. The condition is illustrated in the lower left-hand region of (c).

opportunities is what we call multistep filtration (Mechanism 3). Planova filters have thick functional layers for Mechanism 3, and are very different from membranes structured to remove viruses with extremely thin skin functional layers reported by Bolton et al.[3] and Bakhshayeshi et al.[4] The contribution of Mechanism 3 may be different in thick and thin functional layers. Planova filters having thick functional layers are a kind of deep filtration. According to Herzig et al.,[8] large particles (diameter above 30 μm) are captured mechanically and small particles (diameter about 1μm) are captured physicochemically in deep filtration. However, viruses of nanosized particles can be captured by size exclusion of mechanical mechanism in Planova filters.

Until now, static factors in virus removal of Planova filters, such as Mechanisms 1 and 3, have been the focus of many studies. However, no report has discussed virus removal membranes through a dynamic perspective such as the flow of the solution inside the membrane and Brownian motion of viruses. For example, Planova filters are usually operated in dead-end filtration mode under constant pressure. Under these filtration conditions, the flow of the solution inside the membrane changes with the filtration pressure. This, in turn, may potentially influence the behavior of the viruses. Moreover, as Planova filters mainly target viruses with diameters of tens of nanometers, the Brownian motion of these viruses cannot be ignored. Focused on particle removal by porous media not designed for virus removal, previous literatures discussed removal mechanism through a dynamic perspective. Bowen and Sharif.[9] studied particle-size exclusion mechanism in membranes and considered hydrodynamic forces, electrostatic forces, and Van der Waals forces. Kim and Zydney[10] studied the Brownian motion of particles within a membrane. In addition to Brownian motion, they also considered hydrodynamic forces and electrostatic forces from a dynamic perspective. Bowen and Sharif and Kim and Zydney focused on mainly electrostatic forces. However, as electrolyte concentration is generally high in the set of solutions targeted by virus removal membranes (~50–150 mM), the effects of electrostatic forces on these membranes are typically negligible.

In this study, we concentrated on solution flow and virus movement and proposed constraint by hydrodynamic forces (Mechanism 2) as a dynamic factor. Even if a virus is prevented by a size excluding capillary from moving farther downstream, it is still ceaselessly moving due to Brownian motion. These post exclusion virus movements are also very important in virus removal. Some constraining force is necessary to hold the moving virus at the capillary entrance. In filtrations using adsorption, this role is filled by attractive forces acting between the viruses and the membrane walls. However, in filtrations using Planova filters, this role is filled by hydrodynamic forces because the contributions of surface interactions (e.g., electrostatic forces, etc.) are negligible. Figures 1a, b show two possible outcomes for the constraint of viruses by hydrodynamic forces near the entrance of the small capillary and Figure 1c illustrates how virus behavior is regulated by size exclusion and constrained by hydrodynamic forces. When the flow velocity is high and the capillary is small enough for size exclusion, as shown in Figure 1a and in the upper left-hand region of Figure 1c, the flow overcomes the Brownian motion of the viruses and they can be held near the entrance of the small capillary. In short, viruses can be strongly constrained when flow velocity is high. In this study, viruses under the conditions shown in Figure 1a are referred to as "captured." In contrast, when the flow velocity is low and the capillary is small enough for size exclusion, as shown in Figure 1b and in the lower left-hand region of Figure 1c, the viruses are only weakly constrained and their ranges of motion are widened. In this study, viruses under the conditions shown in Figure 1b are referred to as "drifting." When a virus is drifting, it could potentially encounter another capillary connected to the void it occupies. If the virus encounters a small capillary, it will again be size excluded and will remain in the void. On the other hand, if the virus encounters a large capillary, it is able to pass on into the next void (see the dotted arrow in Figure 1b). If the virus does drift into the next void, it may be captured by the next capillary it encounters (Mechanism 3). However, there is a possibility that it may instead pass through that capillary as well and so continue downstream. As capillaries come in a range of sizes, a fraction of the drifting viruses will move stochastically downstream. Virus drifting due to weak virus constraint leads to decreases in virus removal capability. For reliable virus removal, viruses must be captured by the strong constraint shown in Figure

1a. Predictably, when filtration flux and flow velocity are low, the fraction of drifting viruses increases and the membrane's virus removal capability decreases.

In addition to considering two known static mechanisms (Mechanisms 1 and 3), we also investigated new dynamic factors (solution flow and virus movement), detailed a proposed virus removal mechanism (constraint by hydrodynamic forces: Mechanism 2), and verified our proposition experimentally. We performed virus behavior simulations, virus removal experiments, and virus removal simulations. As the virus concentrations in the filtrates produced by these commercial filters are usually below the detection threshold, experimental study of their virus removal capabilities is limited. In the study, we present here, the virus removal mechanism in Planova filters was analyzed by means of experimental analysis and numerical simulation. Finally, the results of the studies are discussed in terms of the relationship between microscopic mechanisms and macroscopic virus removal capabilities.

Theory

We proposed constraint by hydrodynamic forces (Mechanism 2), which are dependent on the velocity of the solution. In this study, we define critical flow velocity (U_{cr}) as the flow velocity threshold above which small capillaries are able to capture viruses. If the average flow velocity in a capillary (u) is higher than the critical flow velocity ($u \geq U_{cr}$) and the capillary is small enough for size exclusion, a virus can be constrained at the capillary's entrance such that its range of motion will not extend to other capillaries connected to the same void. U_{cr} depends on the specific shape of the capillaries and the voids, and therefore it must be determined empirically.

The relationship between hydrodynamic forces and Brownian motion can be evaluated using the Peclet number expressed in Eq. 1 below[11]

$$\mathrm{Pe} = \frac{u d_{\mathrm{virus}}}{D} \tag{1}$$

where u is the average flow velocity inside a capillary, D is the diffusion coefficient defined as $D = kT/(3\pi\eta d_{\mathrm{virus}})$, where η is the viscosity of the solvent, and d_{virus} is the diameter of the virus. If Pe $>>$ 1, convection is predominant and diffusion is negligible. On the other hand, if Pe $<<$ 1, diffusion is predominant and convection is negligible. Virus capture conditions independent of virus size and solution properties are not expressed in a critical flow velocity value but rather in a critical Peclet number (Pe_{cr}), as shown in Eq. 2

$$\mathrm{Pe}_{cr} = \frac{3\pi\eta U_{cr} (d_{\mathrm{virus}})^2}{kT} \tag{2}$$

The critical Peclet number that is the threshold above which hydrodynamic forces overcome Brownian motion was expected to be approximately 1.

Hydrodynamic forces do not hold a captured virus entirely still. Rather, they constrain the virus to the area near the capillary entrance, as shown in Figure 1a. This is very important to understand the virus capture capacity of each capillary. In the general conception of size exclusion, whenever a capillary captures a single virus, the virus plugs the capillary and the flow to that capillary diminishes (complete pore blocking).[3] This means that each capillary can only capture one virus. However, due to the capillary-void structure of Planova filters, the flow to a capillary does not diminish when it has captured a virus. This is because the Brownian motion of the virus keeps it continually moving and prevents it from plugging the capillary. The capillary is then able to capture additional viruses because the flow continues through it even after the first virus has been captured. Supporting this hypothesis, in an experiment using a Planova filter, multiple viruses were found to have collected in a single void.[2] Since virus capture occurs at capillary entrances, each capillary's virus capture capacity is not based on the size of the space inside it but rather on the distance between its entrance and other capillaries directly adjacent to it. It suggests that, a critical parameter for filter construction is the density of capillaries connecting the void space, or rather the ratio of capillaries to voids. The virus capture capacity of a Planova filter consisting of a continuous void and capillary structure is expected to be larger than that of a membrane consisting only of a continuous thin capillary structure.

Virus Behavior Simulation

To microscopically examine the validity of Mechanism 2, virus behavior simulations were performed.[12] Viruses were equated to hard spherical particles. The Langevin equation that we used to describe the Brownian motion of the particle and the frictional resistance between the particle and the fluid is expressed in Eq. 3 below

$$\frac{d\mathbf{v}}{dt} = -\zeta'(\mathbf{v} - \mathbf{v}_{\mathrm{solvent}}) + \frac{1}{m'}\mathbf{F^B} \tag{3}$$

where $\zeta' = \frac{3\pi\eta d_{\mathrm{particle}}}{m'}$, m' (the apparent mass) $= m + \frac{\pi (d_{\mathrm{particle}})^3 \rho_{\mathrm{solvent}}}{12}$, $\mathbf{v}$ is the velocity of the particle, d_{particle} is the diameter of the particle, m is the mass of the particle, $\mathbf{v}_{\mathrm{solvent}}$ is the flow velocity of the solvent, ρ_{solvent} is the density of the solvent, η is the viscosity of the solvent, and $\mathbf{F^B}$ is the random force acting on the particle due to Brownian motion. $m'\zeta'$ is the friction coefficient.

By integrating Eq. 3, particle velocity ($\mathbf{v}$) and particle position ($\mathbf{r}$) can be expressed in the following respective equations

$$\mathbf{v}(t+\Delta t) - \mathbf{v}(t) = -(\mathbf{v}(t) - \mathbf{v}_{\mathrm{solvent}})\left(1 - \mathrm{e}^{-\zeta'\Delta t}\right) + \delta\mathbf{v}^{\mathrm{B}} \tag{4}$$

$$\mathbf{r}(t+\Delta t) - \mathbf{r}(t) = \frac{1}{\zeta'}(\mathbf{v}(t) - \mathbf{v}_{\mathrm{solvent}})\left(1 - \mathrm{e}^{-\zeta'\Delta t}\right) + \mathbf{v}_{\mathrm{solvent}}\Delta t + \delta\mathbf{r}^{\mathrm{B}} \tag{5}$$

$\delta\mathbf{r}^{\mathrm{B}}$ and $\delta\mathbf{v}^{\mathrm{B}}$ are the terms which depend on Brownian motion. They were determined randomly to follow two-dimensional (2-D) normal distribution (see Appendix). Equations 4 and 5 were solved by time development to determine particle velocity and position. Computer simulation code in C++ was developed to solve Eqs 4 and 5. The physical conditions of the simulation are shown in Table 1. For this simulation, a model of a void and its capillary entrances was made by erecting a virtual wall at $y = 0$. Uniform flow was

Table 1. Virus Behavior Simulation Conditions

Parameter	Value
d_{virus}	21 nm
m	$\rho_{\mathrm{solvent}} \cdot \pi d_{\mathrm{virus}}{}^3/6$
ρ_{solvent}	1 g/cm^3
T	293 K
η	1 mPa s
$\lvert \mathrm{v}_{\mathrm{solvent}} \rvert$	1E-4 to 1E-2 m/s

then input at a perpendicular angle to this wall. The space in the model corresponds to the void and the wall corresponds to the size excluding capillary entrances. The solution could pass through the wall with no flow resistance; the viruses, however, could not pass through the wall and it was assumed that they were specularly reflected by it. It was also assumed that the flow was not affected by virus movement and thus the flow velocity was held constant. One particle was set to initially contact the wall at $(x, y) = (0 \text{ nm}, 10.5 \text{ nm})$ at $t = 0$. This simulation was implemented at various flow velocities.

Experiment

Model virus removal membrane

Model hollow fiber membranes were manufactured from hydrophilized polyvinylidene fluoride according to the methods of Nagoya and Koguma[13] and Koguma and Nagoya.[14] Total thickness was 66 μm and average capillary diameter was 23.5 nm. The model membranes were bundled and used to prepare a filter with an effective surface area of 0.001 m^2. The capillary diameters of these model membranes were regulated such that post filtration virus concentrations could be detected. The average capillary diameter of the membrane can be determined by the water flow method[15]

$$d_{\text{cap,avg}} = \sqrt{\frac{32\eta_w LU}{\varepsilon \Delta P}} \tag{6}$$

where η_w is the viscosity of water, L is the thickness of the membrane, U is the apparent velocity, and ε is the porosity of the membrane. However, the porosity of the model membrane after hydrophilization could not obtain accurately, and the average capillary diameter of the membrane could not be determined directly by Eq. 6. As the water flux of laminar flow was proportional to average capillary diameter to the power four, we estimated the capillary diameter by the following equation in this study

$$\frac{J_H}{J_B} = \frac{{d_H}^4}{{d_B}^4} \tag{7}$$

where J_H is the water flux of the membrane after hydrophilization, J_B is the water flux before hydrophilization, d_H is the average diameter of the membrane after hydrophilization, and d_B is the average diameter of the membrane before hydrophilization. d_B was determined by Eq. 6. It is noticed that d_H is not a real pore size of this model membrane but conveniently calculated to use in this simulation. This pore size is estimated as cylindrical pore and not directly expressed the pore which contribute virus capture in a single-layer membrane. This value is changed with pore structure of membrane.

Preparation of virus solution

Porcine parvovirus (PPV; 90HS strain, Japanese Association of Veterinary Biologics, Japan) was propagated in PK-13 (ATCC No.CRL-6489) cells at 37°C. The growth medium was Dulbecco's modified Eagle's medium (D-MEM) with 1000 mg/L of D-Glucose and 584 mg/L of L-Gln (Nikken Seibutsu Igaku Laboratory, Japan) containing 3% fetal bovine serum (FBS). Serum-free PPV was obtained from the supernatant after exchanging to a medium without FBS before cytopathic effects appeared in the inoculated host cells. The supernatant was collected and centrifuged at 4°C at 3000 rpm for 20 min to pellet cell debris. Then, the supernatant was filtered using a 0.45-μm filter (surfactant-free cellulose acetate: SFCA 50-mm diameter membrane, Nalgene Nunc International, USA). The concentration of the serum-free PPV stock solution was about $10^{8.5}$ $TCID_{50}$ (median tissue culture infectious dose)/mL.

Preparation of protein solution

We used polyclonal human IgG (Venoglobulin®-IH, Benesis Corporation) as the model antibody. The original solution contained 50 mg/mL IgG and 50 mg/mL sorbitol as the stabilizer. This solution was diluted with D-MEM with 1000 mg/L of D-Glucose and 584 mg/L of L-Gln (Nikken Seibutsu Igaku Laboratory) until it reached the final IgG concentration of 10 mg/mL.

Preparation and filtration of solutions with various viscosities

Zero weight percent and 2.5 wt % polyethylene glycol 20,000 (PEG; Wako)/PBS (phosphate buffered saline) (Dulbecco's PBS[–], Nittsui Seiyaku) solutions were prepared. Measurements of solution viscosity were taken during validation using an Ostwald viscometer at 25°C. The serum-free PPV described above ($10^{8.5}$ $TCID_{50}$/mL) was spiked into the solutions at 0.5 vol %. Then, a prefiltration was conducted using a Planova 35N filter (0.001 m^2, Asahi Kasei Medical) to remove virus aggregates. To adjust the fluxes of the 0 and 2.5 wt % PEG/PBS solutions to roughly the same amount [~20 L/(m^2 h)], filtrations using the model virus removal membranes described above were conducted at 49 kPa and 25°C for the 0 wt % PEG/PBS solution and at 108 kPa and 25°C for the 2.5 wt % PEG/PBS solution.

Virus assay method

We determined the viral concentrations in samples of the solutions before and after filtration with the $TCID_{50}$ method using PK-13 cells. After a holding period, the viral concentrations of feed solution samples were also determined. We then prepared a 10-fold serial dilution of the samples and inoculated them into cell culture plates. $TCID_{50}$ was calculated using the Reed and Muench method.[16] The virus titers were expressed as $TCID_{50}$/mL. In this experiment, the detection threshold of this method was 0.5 $\log_{10}$ $TCID_{50}$/mL. The decrease in activity in the feed samples after the holding period was found to be negligible. The permeability of the virus is represented by the following equation

$$\text{Pm} = \frac{C_f}{C_o} \tag{8}$$

where C_o is the concentration of the feed solution and C_f is the concentration of the filtrate.

Virus filtration

Dead-end filtrations were performed using the 0.001 m^2 model virus removal filter at filtration pressures of 10, 20, 49, 98, 196, and 294 kPa. The removal rate of PPV from a 10 L/m^2 pool was measured with the $TCID_{50}$ method described above. The flow characteristics of the membrane and the solutions used in the experiments are given in Figure 2. A strong linear correlation between the filtration pressure and the filtration flux was confirmed.

Virus Removal Simulation

We developed a simulation based on our proposed virus removal mechanism to find the virus permeability of the

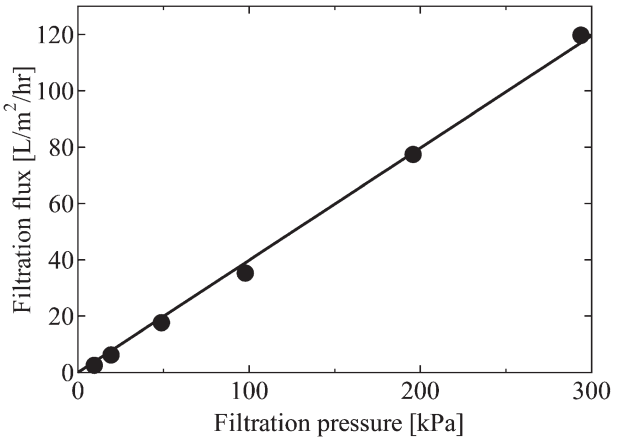

Figure 2. Filtration flux as a function of filtration pressure for the model membrane.

entire membrane. The virus removal simulation was carried out in two stages. The first stage was the network model simulation. A network that imitated the network of capillaries within a membrane was prepared and the localized flow velocity inside each capillary was found. The second stage was the convection-diffusion simulation. The movement of viruses in each localized flow area was calculated, and the virus permeability of the entire membrane was found.

Network model simulation for localized flow velocity

To study Mechanism 2, the localized flow velocity inside each capillary must first be found. The membrane structure, assumed to be spatially uniform and isotropic, was modeled in a 3-D network with the voids as nodes and the capillaries as links (Figure 3a). Flow analyses of porous media using similar network models were reported first by Fatt[17] and more recently, by Zhao et al.[18] and Zhu et al.[19] However, only the total flow resistances of the membranes were studied in these reports; the flow velocities in localized regions (such as capillaries) were not discussed. On the other hand, the localized flow velocity inside each capillary is very important to our proposed virus removal mechanism. Although our study used models similar to those used before, unlike the previous reports, we applied them to localized areas. We took capillary size distribution and connectivity between voids into account and calculated the flow velocity in each capillary with great detail. In our 3-D network, the links did not have uniform diameters. Instead, they had diameters of varying sizes like the capillaries in actual membranes. Simulated multistep filtration through these links of varying diameter yielded high removal capability. Link diameter distribution was assumed to follow logarithmic-normal distribution and link length was assumed to be uniform.

A 2-D rendering of the network is shown in Figure 3b, and the characteristics of the network are given in Table 2. To create this network model, first, nodes were packed as closely as possible with links connecting each to its neighbors. Next, links were randomly deleted until the average number of links connected to each node was 4. Finally, the diameter of each link was determined randomly using logarithmic-normal distribution. We assumed that the viscosity inside the membrane was constant. This network was then converted into an equivalent electrical circuit, as shown in Figure 3c. The resistance in the link between node-i and node-j is expressed in Eq. 9 below[17]

$$\frac{1}{R_{i,j}} = \left(d_{i,j}\right)^4 \tag{9}$$

where $d_{i,j}$ is the diameter of the link between node-i and node-j. The equation of the preservation of current at each node was derived from Kirchhoff's Law for electric circuits

$$\sum_{\text{node-}i} I_{i,j} = \sum_{\text{node-}i} \Delta V_{i,j}/R_{i,j} = \sum_{\text{node-}i} (V_j - V_i)/R_{i,j} = 0 \tag{10}$$

It was assumed that the resistance in a node was negligible compared with that in a link. The voltage at each inlet was set to $V_{\text{in}} = 1$ and the voltage at each outlet was set to $V_{\text{out}} = 0$. The preservation of current at each part of each node was calculated using the successive overrelaxation (SOR) method and the voltage at each node (V_i) was found. From these results, the total resistance (R_{total}) was obtained. We developed computer simulation code of SOR method in C++ to solve Eq. 10 for each node.

As the flow rate corresponds to the electric current in the equivalent circuit, the following relationship holds true for our calculations

$$\frac{Q_{i,j}}{Q_{\text{total}}} = \frac{I_{i,j}}{I_{\text{total}}} = \frac{\Delta V_{i,j}/R_{i,j}}{\Delta V_{\text{total}}/R_{\text{total}}} \tag{11}$$

where $\Delta V_{\text{total}} = V_{\text{in}} - V_{\text{out}}$ and Q_{total} is obtained from the flow properties shown in Figure 2. When the membrane or solution conditions were changed, Q_{total} was calculated from R_{total} and Figure 2 was used as a standard. Using Eq. 11, the flux in each link ($Q_{i,j}$) was calculated and, in turn, was used to calculate the link's average flow velocity.

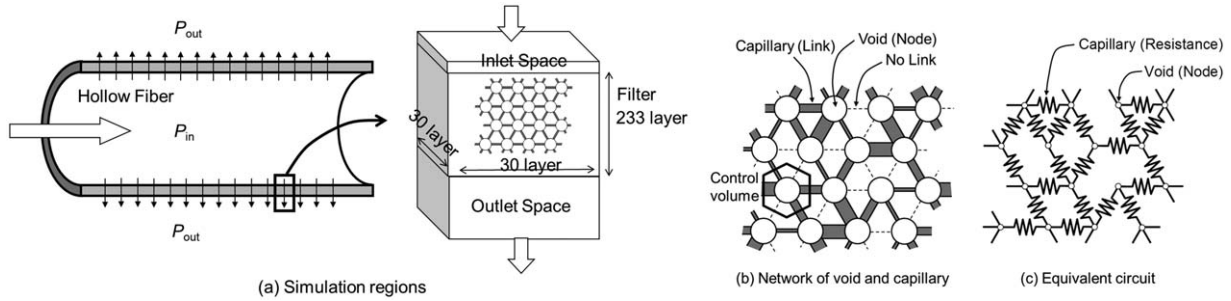

Figure 3. Schematic diagram of simulation regions and 2-D image of network modeling.

Planova filters consist of the follow fiber and are operated in an inside–out mode, where feed solution enters the center of the fiber and is filtered radially through the fiber wall. The fiber wall is the membrane for filtration.

Table 2. Properties of the Model Virus Removal Membrane used for the Simulations

Void diameter	155 nm
Capillary length	124 nm
Number of layers	233
Average connectivity [(total number of capillaries)/(total number of voids)]	4
Capillary diameter (d_{cap})	Log-normal distribution ($d_{cap,avg}$ = 23.5 nm, CV = $\sigma/d_{cap,avg}$ = 1.0)
Volume of inlet space and outlet space	Inlet (S_{in}): 0.082 L/m^2 Outlet (S_{out}): 7.5 L/m^2

Convection-diffusion simulation for virus removal

Assuming that the viruses existed in the protein solution as solutes, we focused only on them for this simulation. We did not consider flow resistance increase by virus capture or virus capture capacity to instead examine initial virus removal capability. The following virus convection-diffusion equation was solved for the network and the localized flow velocities described above

$$\frac{\partial C}{\partial t}+\left[u\cdot\frac{\partial C}{\partial x}\right]_{d_{cap}\geq d_{virus}}-\left[D_{eff}\cdot\frac{\partial^2 C}{\partial x^2}\right]_{d_{cap}\geq d_{virus}}+S=0 \quad (12)$$

where C is the virus concentration within a void, D_{eff} is the effective diffusion coefficient of the present network model, and u is the average flow velocity in a link connecting two nodes (previously obtained). Convection and diffusion can only occur when $d_{cap}\geq d_{virus}$ and not when $d_{cap}<d_{virus}$ because viruses cannot pass through capillaries with diameters smaller than their own. Accordingly, the convection term and the diffusion term in Eq. 12 both have a limiting factor. Also, because virus capture occurs in the convection that happens when the conditions for size exclusion and constraint by hydrodynamic forces are met, a virus loss term (S) is included in Eq. 12. S is expressed in the following equation

$$S=\left[u\cdot\frac{\partial C}{\partial x}\right]_{d_{cap}<d_{virus},|u|\geq U_{cr}} \quad (13)$$

This microscopic virus removal mechanism was reflected in a macroscopic simulation. Patanker's concept of control volume was used for space discretization of Eq. 12.[20] The space within one node and in half of the length of each link connected to it was identified as the control volume. A 2-D image of the control volume is shown in Figure 3b. The convection term and the diffusion term in Eq. 12 were discretized by integrating the direction of every link connected to the node into the control volume. The interface area between control volumes was a cross-section of the connecting links. The Euler explicit method was used to discretize the time term in Eq. 12. We developed computer simulation code in C++ to solve Eq. 12 for every void.

Feed and filtrate membrane sides with the same amount of space as those used in the experiments were established (called S_{in} and S_{out}, respectively). Viruses were assumed to be perfectly mixed within those spaces. The links in the network were connected to apply periodic boundary conditions to the direction perpendicular to filtration. Initially, virus concentration (C) was set to zero at every point. In conjunction with the experiments, the virus concentration of the feed solution was set to C_{in} = 1.6E12 virus/L. The changes in the virus concentrations in the feed side, in the filtrate side, and in each node were obtained through a time-development simulation.

Results and Discussion

Local virus behavior

To examine the effects of hydrodynamic forces and Brownian motion on virus behavior, we carried out microscopic virus behavior simulations at various flow velocities (u). The changes in the central locations of simulated viruses within a period of 1E-4 s at flow velocities of 1E-2 m/s, 1E-3 m/s, and 1E-4 m/s are plotted in Figures 4a–c, respectively. The trajectories taken by each of the three viruses simulated in each of the three trials are, respectively, indicated by a thin solid line, a thick solid line, and a dotted line. The random movements of the viruses due to Brownian motion were observed. At the flow velocity of 1E-2 m/s, the viruses were held strongly against the wall and hardly left it, as shown in Figure 4a. This was caused by the constraint by hydrodynamic forces shown in Figure 1a. When the flow velocity is high, as it was in this case, even if a virus moves due to Brownian motion, it will be constrained by hydrodynamic forces at the entrance to a small capillary. Additionally, we know that convection is dominant at u = 1E-2 m/s because it corresponds to Pe = 10. Therefore, this flow velocity is sufficiently high to constrain viruses. At the flow

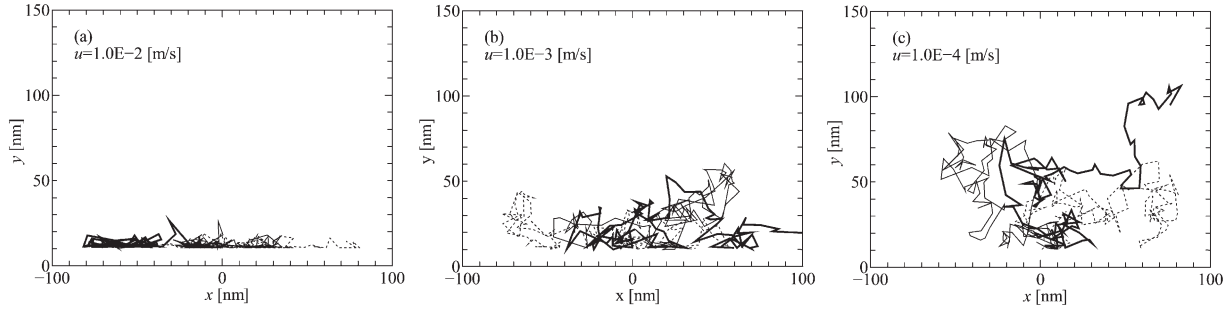

Figure 4. Simulated trajectories of viruses at different flow velocities.

Three runs were done for each flow velocity. These runs are individually represented by a thin solid line, a thick solid line, and a dotted line.

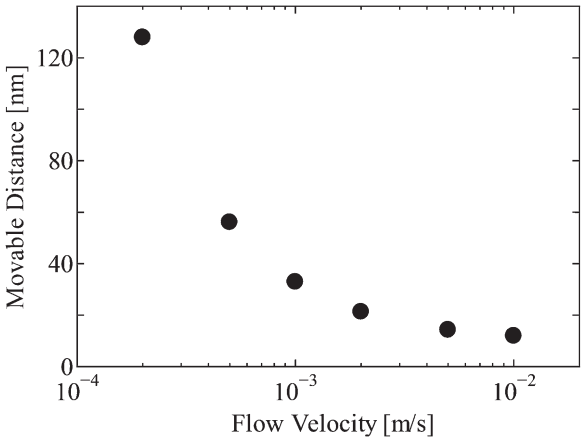

Figure 5. Simulated movable distances of viruses as a function of flow velocity.

velocity of 1E-3 m/s, shown in Figure 4b, the viruses had a significantly wider range of movement than those in Figure 4a. Furthermore, at the flow velocity of 1E-4 m/s, the viruses could basically move around freely, as shown in Figure 4c. This situation was similar to that shown in Figure 1b. When the flow velocity is low, as it was in this case, even if viruses are near small capillaries capable of size exclusion, they are still able to freely move around and are not constrained.

When the observations of virus behavior were lengthened, the average distance of the viruses from the walls converged to a certain value for each flow velocity. This average distance (y) gives the range in which a virus can move freely at that flow velocity (Figure 5). This is also called a virus' "movable distance" (L_m). As the flow velocity increases, the movable distance decreases. For example, when $u = 2E\text{-}4$ m/s, L_m is 128 nm. As this distance is similar to the average void size of 155 nm, the viruses are not constrained and are able to move freely throughout almost the entire void at this flow velocity. When $u = 1E\text{-}3$ m/s, L_m is 33 nm. As this distance is similar to the approximate virus size of 21 nm, the viruses can only move a small amount and can largely be constrained at this flow velocity. We approximate that the threshold flow velocity for virus constraint (U_{cr}) lies between $u = 2E\text{-}4$ m/s and $u = 1E\text{-}3$ m/s.

In this simulation, we did not establish limits for virus movement parallel to the wall (i.e., in the x direction). In the experimental membranes, the areas around the capillary entrances are uneven and get gradually thinner. If a virus was strongly constrained near one of these entrances, it could barely move in the x-direction as there would be a void wall there to block its path (Figure 1a). On the other hand, if the virus was only weakly constrained and could move about freely, there would be no wall directly barring the x-direction and the virus would be able to move that way also (Figure 1b). This would lead to a decrease in the virus capture capability of the membrane because the virus would have the potential to encounter other large capillaries during this free movement.

Virus behavior was simulated microscopically, and the effects of hydrodynamic forces and Brownian motion on localized membrane areas were investigated. Through this, we demonstrated that the Brownian motion of viruses cannot be ignored, we clarified the effects of constraint by hydrodynamic forces, and we showed the potential of our proposed mechanism at a microscopic level.

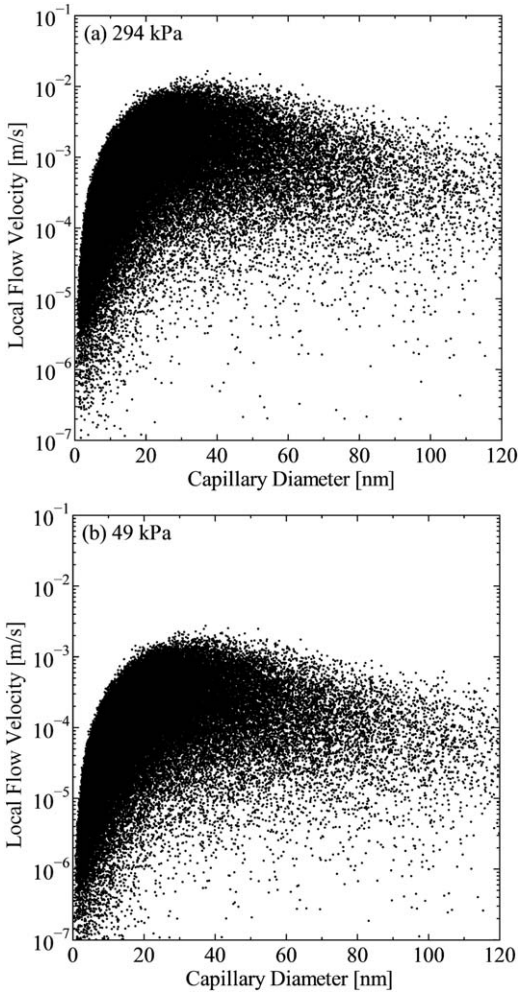

Figure 6. Simulated localized flow velocities of capillaries at varying filtration pressures.

Localized flow velocity

In the previous section, we demonstrated that, at low flow velocities, viruses are moved by Brownian motion and cannot be captured even by capillaries with diameters much smaller than their own. In this section, we discuss the simulated localized flow velocity in each capillary. As the capillaries vary in diameter and are connected in a network, the velocities in the capillaries also vary. Capillaries of the same size do not necessarily have the same flow velocity. The localized flow velocity of each capillary was calculated in the first stage of the virus removal simulation. Figure 6 plots the diameter and flow velocity of each capillary at simulated filtration pressures of 49 and 294 kPa. There was a wide range of capillary flow velocities at both filtration pressures. As the flow velocity ranges fell inside the approximate threshold flow velocity range for virus constraint described in the previous section ($u = 2E\text{-}4$ m/s to $u = 1E\text{-}3$ m/s), it is clear that the phenomenon described above also occurs at each localized membrane area. Thus, the validity of our proposed mechanism is confirmed in this microscopic perspective. As expected, when the filtration pressure increases, the flow velocity ranges, the number of capillaries able to capture viruses, and the virus removal rates also increase.

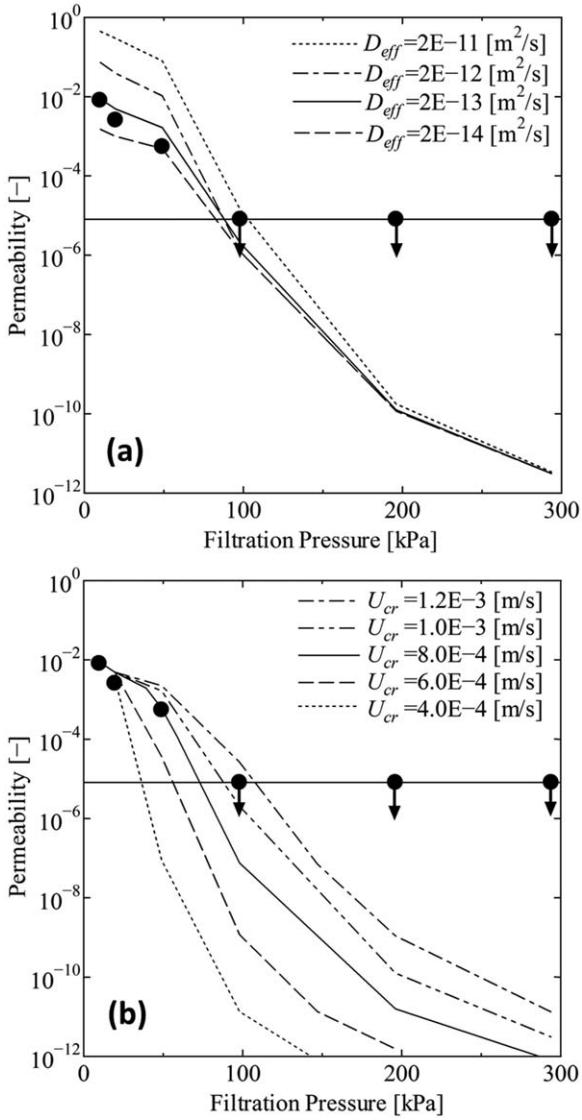

Figure 7. Experimental and simulated results of PPV permeability (a) at various effective diffusion coefficients and (b) at various critical velocities.

Each point indicates an experimental result. Each arrow indicates that the virus concentration of the filtrate was below the detectable level.

Effect of localized flow velocity on virus removal

The phenomena of hydrodynamic forces and Brownian motion can be evaluated using the variable Pe shown in Eq. 1. To investigate how flow velocity, a factor of Pe, affects virus removal capability, we performed experiments at various filtration pressures. The results of the experiments are shown in Figure 7a, a graph of the permeability of PPV with respect to filtration pressure. Symbol plots are experimental results and lines are simulated results, as mentioned below. The arrows in Figure 7a indicate that the virus concentration of the filtrate was below the detection threshold and that the permeability was higher than the plotted value. Our results show that virus permeability is dependent on filtration pressure. As filtration pressure decreases, virus permeability increases. This is because decreases in filtration pressure cause decreases in localized flow velocities which, in turn, cause increases in the occurrences of the conditions shown in Figure 1b.

When filtration pressure was above 98 kPa, virus concentrations were below the detection threshold. This made it difficult to discuss the virus removal capability of the membrane in detail with only the experimental data. Accordingly, we then performed a number of virus removal simulations at various filtration pressure conditions. The simulation conditions matched the experiment conditions; we used PPV (21 nm) as the virus and calculated the virus permeability at 10 L/m^2.

There are two simulation methods for analyzing virus movement within a network: Lagrangian and Eulerian. A Lagrangian simulation would be very hard to perform on our system because the virus concentrations in our filtrates are around 1/10,000 of those in our feed solutions, meaning that the number of trials required would be enormous. Therefore, an Eulerian simulation was used instead and the virus concentration at each membrane area was found.

Because the effective diffusion coefficient of the virus in the present network model (D_{eff}) and the critical flow velocity for virus capture (U_{cr}) are dependent on solution properties and the specific shapes of capillaries and voids, they must be determined empirically. The results of simulations performed at varying D_{eff} values and a constant U_{cr} value of 1E-3 m/s are shown as lines in Figure 7a. When filtration pressure was low, D_{eff} had an effect on virus permeability. This is because diffusion gains dominance when flow velocities slow due to decreases in filtration pressure. The experiment and simulation results agreed when $D_{\mathrm{eff}} = 2\text{E-}13$ m^2/s. If we assume a virus is a spherical particle 21 nm in diameter, we could estimate its diffusion coefficient in free space to be 2E-11 m^2/s. The effective diffusion coefficient obtained with the experiment and simulation results was 1/100 of the diffusion coefficient in free space. After this, $D_{\mathrm{eff}} = 2\text{E-}13$ m^2/s was used for all following simulations. The results of varying the U_{cr} are shown in Figure 7b. They show that as U_{cr} increases, the permeability increases significantly for a given pressure. The simulation and experiment results agreed when $U_{\mathrm{cr}} = 8\text{E-}4$ m/s. This is consistent with the critical flow velocity range approximated by our microscopic virus behavior simulation (2E-4 to 1E-3 m/s). Also, this corresponds to $\mathrm{Pe}_{\mathrm{cr}} = 0.8$. When $\mathrm{Pe} > \mathrm{Pe}_{\mathrm{cr}}$, hydrodynamic forces overcome Brownian motion and viruses can be captured (Figure 1a). $\mathrm{Pe}_{\mathrm{cr}}$ is the threshold of virus capture and obtained $\mathrm{Pe}_{\mathrm{cr}}$ is close enough to 1 that the competing phenomena of hydrodynamic forces and Brownian motion could occur. This result supported our proposed mechanism. $\mathrm{Pe}_{\mathrm{cr}} = 0.8$ was used for all following simulations.

These experiments clarified the effects of filtration pressure on virus permeability. The results of the experiments were consistent with the results of the simulations based on our proposed mechanism. Filtration pressure affects virus permeability because it affects the localized flow velocity in every capillary. This phenomenon is explained by our new Mechanism 2. When filtration pressure is high, flow velocities throughout the membrane are high and the conditions shown in Figure 1a are dominant. As filtration pressure decreases, however, the amount of capillaries with flow velocities beneath U_{cr} increases and the conditions shown in Figure 1b become more dominant. Thus, it is clear that filtration pressure affects not only processing time but also virus removal capability.

Effect of diffusion coefficient on virus removal

To investigate how the diffusion coefficient, another factor of Pe in Eq. 1, affects virus removal capability, experiments and simulations were carried out using solutions of varying viscosities (η). Viscosity is typically inversely proportional to the diffusion coefficient. Solution viscosity was regulated using PEG. A set filtration pressure was determined to keep filtration flux, and thus localized flow velocities, constant despite the variations in viscosity (Table 3). As flow velocity was held constant, these experiments examined only the effects of solution viscosity. The filtration fluxes estimated from the flow properties shown in Figure 2 and the viscosities shown in Table 3 were used in the simulations. The viscosity of the protein solution used in the fluid flow experiments shown in Figure 2 was 0.97 mPa s. The U_{cr} at each viscosity, obtained using $Pe_{cr} = 0.8$, is also shown in Table 3. When viscosity doubles, U_{cr} is halved. As viscosity increases, the Brownian motion of the viruses decreases and the viruses can be constrained by lower flow velocities.

The experiment and simulation results are given in Table 3. They show that virus permeability decreases as viscosity increases. The experiment results correspond with the trend shown in the simulation results. As the effects of viscosity on virus permeability could not be caused only by the static size exclusion mechanism, the data suggest that our mechanism of constraint by hydrodynamic forces is effective. The virus permeability of the simulation was less than that of the experiment. We expect that this was why viscosity of the solution of high-molecular-weight solute (PEG) was not perfectly inversely proportional to the diffusion coefficient. These experiments and simulations clarified the effects of solution viscosity on virus permeability. At a constant flow velocity, viruses are more strongly constrained when viscosity is higher.

The results of the previous section show the effects of changes in flow velocity, and the results of this section show the effects of changes in viscosity (diffusion coefficient). Flow velocity and diffusion coefficient are factors of Pe (Eq. 1). The relationship of permeability and macroscopic Pe calculated by Eq. 1, where the apparent macroscopic flow velocity is used for u, is shown in Figure 8, including the results of previous section and this section. They show that virus permeability decreases as Pe increases and virus removal can be evaluated using Pe. Thus, the validity of our proposed mechanism is confirmed in this macroscopic perspective of virus removal capability. This suggests the importance of solution conditions in relation to virus removal capability. Depending on conditions, temperature changes can also have an effect on the diffusion coefficient.

Effect of virus size and capillary size on virus removal

To this point, we have used PPV (21 nm) as our model virus for these experiments. In this section, we investigate the influence of virus size using computer simulations. Virus size, the last remaining factor of Pe in Eq. 1, also affects size exclusion. As virus size changes, the diffusion coefficient and the critical flow velocity at which viruses can be strongly constrained also change. The relationship between virus size and critical flow velocity, determined using the critical Peclet number ($Pe_{cr} = 0.8$), is shown in Figure 9. As virus size decreases, critical flow velocity increases. The capture of small particles needs high velocity. This is very important for virus removal processes of separation of viruses and proteins. Figure 10 shows the results of simulations conducted at 49 and 294 kPa with viruses of various sizes. As virus size increases, virus permeability decreases. Therefore, large viruses are less permeable than small viruses because their increased size makes them more susceptible to size exclusion and constraint by hydrodynamic forces. The virus size at which permeability begins drastically rising is approximately 15 nm at 294 kPa and approximately 19 nm at 49 kPa. When filtration pressure is higher, smaller viruses can be removed. Therefore, filtration pressure affected virus removal capability in this simulation the same way as described above.

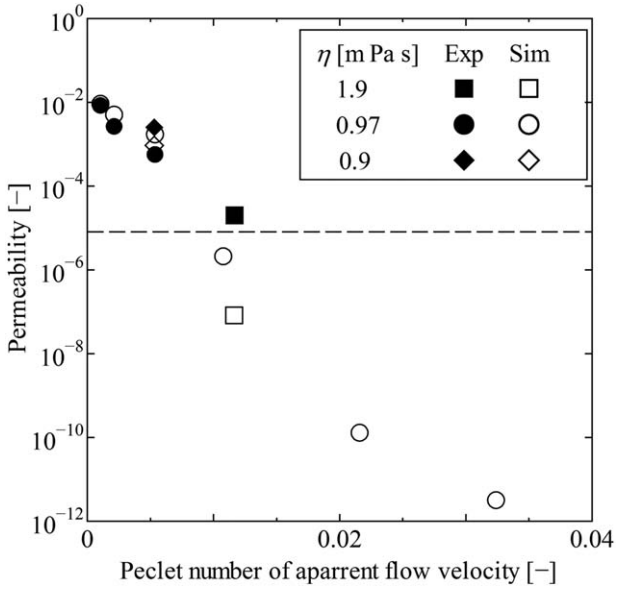

Figure 8. Simulated and experimental results of PPV permeability at various conditions.

The detectable level is indicated by the horizontal broken line.

Although proteins are smaller than viruses, they can also be removed by the same mechanisms. IgG (10 nm) was used as the protein in our simulations and the results show 99% protein permeability. This result is consistent with the approximately 100% IgG permeability (recovery rate) shown by the experiments.

Next, we focused on capillary diameter, another factor of the size exclusion mechanism. It was very difficult to create a membrane with controlled capillary diameters without changing its essential structure. Additionally, the virus concentrations of filtrates produced by membranes created with

Table 3. Properties of PEG Solution and Experimental and Simulated Permeability

PEG Density (vol %)	Viscosity (mPa s)	Filtration Pressure (kPa)	Critical Flow Velocity (m/s)	Permeability (–)	
				Experiment	Simulation
0	0.90	49	8.6E-4	2.5E-3	9.3E-4
2.5	1.90	108	4.1E-4	2.0E-5	7.9E-8

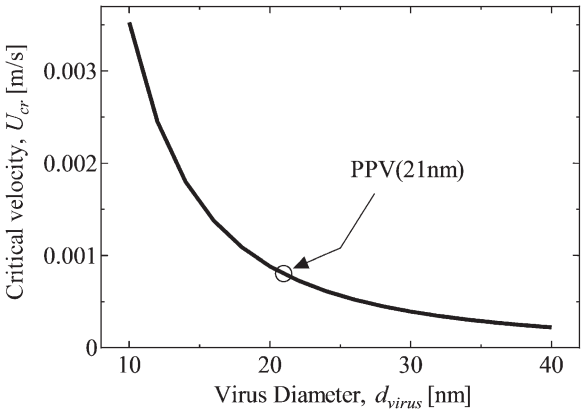

Figure 9. Critical flow velocity as a function of virus size.

This is derived from $Pe_{cr} = 0.8$.

solely small capillaries were below the detection threshold. Therefore, we examined the effects of average capillary diameter using simulations. We assumed that the parameters other than the average capillary diameter were constant and set $Pe_{cr} = 0.8$ and CV (coefficient of variation of pore size) $= \sigma/d_{cap,avg} = 1.0$. The filtration flux used in the simulation was obtained from Figure 2 and Eq. 7. The results of the simulations of PPV virus at filtration pressures of 294 and 49 kPa are shown in Figure 11. The results show that PPV permeability decreases as average capillary diameter decreases in both filtration pressures. Decreases in capillary diameters cause increases in size exclusion. However, they also bring about decreases in constraint by hydrodynamic forces by also causing decreases in the flow velocities the capillaries can manage at constant pressure conditions. As the average capillary diameter decreases, these two different effects occur simultaneously. However, it is clear that the effects of the increase of size exclusion are stronger because PPV permeability decreases as average capillary diameter decreases. Thus, even considering the effects of constraint by hydrodynamic forces, we must conclude that size exclusion is the most important factor for virus removal.

Conclusions

This study investigates the virus removal mechanisms of Planova filters, focusing especially on looking at virus movement through a dynamic perspective. We also discuss the

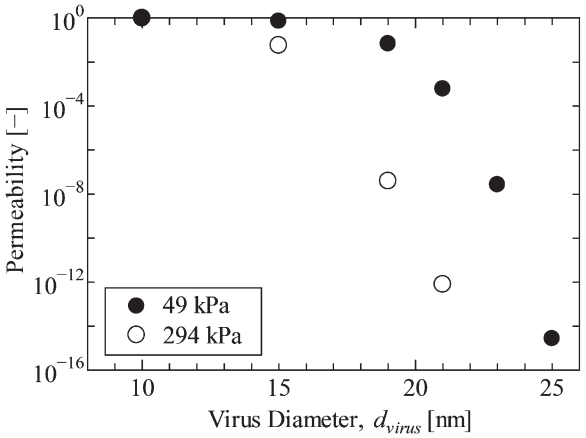

Figure 10. Simulated effect of virus size on permeability at varying filtration pressures.

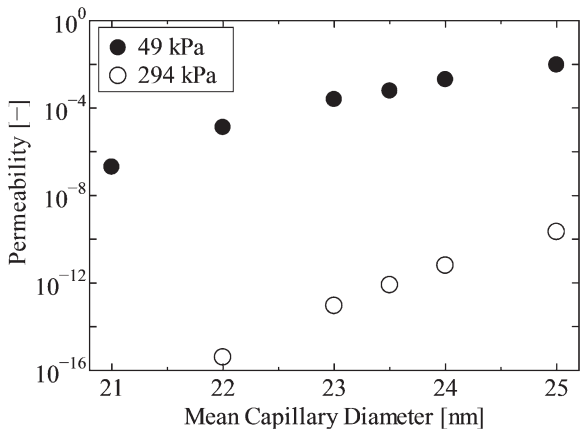

Figure 11. Simulated effect of average capillary diameter on permeability at varying filtration pressures.

Here, $Pe_{cr} = 0.8$ and CV = 1.0.

microscopic virus removal mechanisms of the localized areas of the membrane, the macroscopic virus removal capability of the entire filter, and the relationship between them. We performed localized area virus behavior simulations using the Langevin equation, virus removal experiments using model membranes, and virus removal simulations using network models. The virus removal simulation we developed was based on microscopic virus removal mechanisms and yielded results similar to those of experiments. These simulations were very useful as experiment replacements for cases in which the virus concentration of a filtrate was below the detection threshold, a common problem among virus removal filters.

The virus removal mechanisms of Planova filters are:

1. Size exclusion,
2. Constraint by hydrodynamic forces, and
3. Multistep filtration.

The membrane structure has hitherto been examined from a static perspective and Mechanisms 1 and 3 have already been studied in detail. In this study, we illuminated Mechanism 2 by looking at it through the dynamic perspective of virus movement. We found that viruses are captured because they are constrained by hydrodynamic forces at the entrances of capillaries with diameters smaller than their own. Mechanism 1 alone is insufficient for virus capture of small viruses given the range of pore sizes tested in this study. Mechanism 1 alone is sufficient for large viruses. The virus movement of hydrodynamic forces and Brownian motion is described by Peclet number. We proposed that a critical Peclet number was a condition of virus constraint. The critical Peclet number for the model membrane used in this study was 0.8. If the local Peclet number at a capillary $\geq$0.8, virus is captured.

The macroscopic phenomena caused by this microscopic mechanism are clear. Virus permeability is dependent on filtration pressure. This is because decreases in filtration pressure cause decreases in localized flow velocities which, in turn, cause decreases in the strength of Mechanism 2. Virus permeability is also dependent on solution viscosity. This is because increases in viscosity cause decreases in virus diffusion coefficients which, in turn, cause increases in the strength of Mechanism 2. Thus, it is clear that virus removal capability does not only depend on membranes and viruses, but also on operation conditions such as filtration pressure and solution conditions such as solution viscosity. This knowledge is extremely important for process design.

There is a possibility that the dynamic mechanism described in this study has an effect even in size exclusion-based virus removal membrane filters other than Planova when the virus and capillary diameters are close to each other. We expect that similar phenomena may be observed in the virus removal capabilities of these other filters as well.

Acknowledgment

The authors would like to thank Akiyo Kajitani of the Asahi Kasei Medical Co., Ltd. Bioprocess Division's Technology Development Department for her support of these virus filtration experiments, Christy Scriba of the Asahi Kasei Bioprocess for her helping with the translation, Daniel Strauss of the Asahi Kasei Bioprocess for his scientific reviewing, and Dr. Kazuo Okuyama and Shoichi Ide for their support and continuing interest.

Notation

Variables

C = concentration
D = diffusion coefficient
D_{eff} = effective diffusion coefficient
d_{B} = average diameter of the membrane before hydrophilization
d_{cap} = diameter of capillary
$d_{\mathrm{cap,avg}}$ = average capillary diameter
d_{H} = average diameter of the membrane after hydrophilization
d_{virus} = diameter of virus
$\mathbf{F}^{\mathrm{B}}$ = random force by Brownian motion
I = electric current at a link
J_{B} = water flux of the membrane before hydrophilization
J_{H} = water flux of the membrane after hydrophilization
k = Boltzmann constant
L = thickness of the membrane
L_{m} = movable distance
m = mass of virus
P = filtration pressure
Pe = Peclet number
$\mathrm{Pe}_{\mathrm{cr}}$ = critical Peclet number for virus capture
Pm = permeability
Q = flow rate at a capillary
R = electric resistance
S = loss term
$\mathbf{r}$ = position of particle
T = temperature
t = time
U = apparent velocity
U_{cr} = critical flow velocity for virus capture
u = flow velocity in a capillary
V = voltage at a node
$\mathbf{v}$ = velocity of particle
$\mathbf{v}_{\mathrm{solvent}}$ = flow velocity of solvent

Greek letters

$\delta\mathbf{r}^{\mathrm{B}}$ = a term of Brownian motion, see Appendix
$\delta\mathbf{v}^{\mathrm{B}}$ = a term of Brownian motion, see Appendix
ε = porosity of the membrane
η = viscosity of solvent
η_{w} = viscosity of water
ρ_{solvent} = density of solvent

Subscripts

total = entire membrane
in = inlet
out = outlet

Literature Cited

1. Tsurumi T, Sato T, Osawa T, Hitaka H, Hirasaki T, Yamaguchi K, Hamamoto Y, Manabe S, Yamashiki T, Yamamoto N. Structure and filtration performances of improved cuprammonium regenerated cellulose hollow fiber (BMM hollow fiber) for virus removal. *Polym J*. 1990;22(12):1085–1100.
2. Hongo-Hirasaki T, Yamaguchi K, Yanagida K, Hayashida H, Ide S. Effects of varying virus spiking conditions on a virus removal filter Planova 20N in a virus validation study of antibody solutions. *Biotechnol Prog*. 2011;27(1):162–169.
3. Bolton G, Cabatingan M, Rubino M, Lute S, Brorson K, Bailey M. Normal-flow virus filtration: detection and assessment of the end-point in bioprocessing. *Biotechnol Appl Biochem*. 2005;42:133–142.
4. Bakhshayeshi M, Jackson N, Kuriyel R., Mehta A, van Reis R, Zydney AL. Use of confocal scanning laser microscopy to study virus retention during virus filtration. *J Membrane Sci*. 2011;379;260–267.
5. Wickramasinghe SR, Stump ED, Grzenia DL, Husson SM, Pellegrino J. Understanding virus filtration membrane performance. *J Membrane Sci*. 2010;365:160–169.
6. Tsurumi T, Osawa N, Hitaka H, Hirasaki T, Yamaguchi K, Manabe S, Yamashiki T. Structure of cuprammonium regenerated cellulose hollow fiber (BMM hollow fiber) for virus removal. *Polym J*. 1990; 22(8):751–758.
7. Tsurumi T, Osawa N, Hirasaki T, Yamaguchi K, Manabe S, Yamashiki T. Mechanism of removing monodisperse gold particles from a suspension using cuprammonium regenerated cellulose hollow fiber (BMM hollow fiber). *Polym J*. 1990;22(4):304–311.
8. Herzig JP, Leclerc DM, Le Goff P. Flow of suspensions through porous media: application to deep filtration. *Ind Eng Chem*. 1970; 62(5):8–35.
9. Bowen WR, Sharif AO. Hydrodynamic and colloidal interactions effects on the rejection of a particle larger than a pore in microfiltration and ultrafiltration membranes. *Chem Eng Sci*. 1998;53:879–890.
10. Kim MM, Zydney AL. Effect of electrostatic, hydrodynamic, and Brownian forces of particle trajectories and sieving in normal flow filtration. *J Colloid Interf Sci*. 2004;269:425–431.
11. Trilisky EI, Lenhoff AM. Flow-dependent entrapment of large bioparticles in porous process media. *Biotechnol Bioeng*. 2009;104(1): 127–133.
12. Kamiyama S, Satoh A. *Microsimulation of Colloidal Dispersions*. Tokyo: Asakura Publishing Co., 1997;52–58. (Japanese only).
13. Nagoya F, Koguma I. Multilayer microporous membrane. US Patent 7140496, 2006.
14. Koguma I, Nagoya F. Microporous hydrophilic membrane. US Patent 7459085, 2008.
15. Ishikawa G, Hirasaki T, Manabe S, Yamamoto N. Novel determination method of size of virus in solution using cuprammonium regenerated cellulose membrane (BMM). *Membranes*. 1991;16(6):376–386.
16. Reed LJ, Muench H. A simple method of estimating 50% endpoints. *Am J Hyg*. 1938;27:493–497.
17. Fatt I. The network model of porous media III. *Petrol Trans. AIME*. 1956;207:164–181.
18. Zhao F, Landis HR, Skerlos SJ. Modeling of porous filter permeability via image-based stochastic reconstruction of spatial porosity correlations. *Environ Sci Technol*. 2005;39:239–247.
19. Zhu J, Jabini A, Golden KM, Eicken H, Morris M. A network model for fluid transport through sea ice. *Ann Glaciol*. 2006;44:129–133.
20. Patankar SV. *Numerical Heat Transfer and Fluid Flow*. New York: McGraw-Hill, 1980.

Appendix

We determined $\delta\mathbf{r}^{\mathrm{B}}$ and $\delta\mathbf{v}^{\mathrm{B}}$ by 2-D normal distribution[12]

$$\delta\mathbf{r}^{\mathrm{B}}=(r_1,r_2,r_3),\quad \delta\mathbf{v}^{\mathrm{B}}=(v_1,v_2,v_3)$$

$$\rho(r_i,v_i)=\frac{1}{2\pi\sigma_r\sigma_v\left(1-c_{rv}^2\right)^{1/2}}\exp\left[-\frac{1}{2\left(1-c_{rv}^2\right)}\left\{\left(\frac{r_i}{\sigma_r}\right)^2-2c_{rv}\frac{r_i}{\sigma_r}\frac{v_i-\bar{v}_i}{\sigma_v}+\left(\frac{v_i-\bar{v}_i}{\sigma_v}\right)^2\right\}\right]$$

$$\sigma_r^2=\frac{k_{\mathrm{B}}T}{\zeta' 2}\left\{2\zeta'\Delta t-3+4\mathrm{e}^{-\zeta'\Delta t}-\mathrm{e}^{-2\zeta'\Delta t}\right\}$$

$$\sigma_v^2=\frac{k_{\mathrm{B}}T}{m'}\left(1-e^{-2\zeta'\Delta t}\right)$$

$$c_{rv}=\frac{1}{\sigma_r\sigma_v}\cdot\frac{k_{\mathrm{B}}T}{m'\zeta'}\left(1-e^{-\zeta'\Delta t}\right)^2$$

The expressions with random numbers are:

$$v_i=\left(-2\sigma_v^2\ln R_{i,1}\right)^{1/2}\cos 2\pi R_{i,2}$$

$$r_i=c_{rv}\frac{\sigma_r}{\sigma_v}v_i+\left(1-c_{rv}^2\right)^{1/2}\left(-2\sigma_r^2\ln R_{i,3}\right)^{1/2}\cos 2\pi R_{i,4},$$

where $R_{i,1}, R_{i,2}, R_{i,3}$, and $R_{i,4}$ are uniform random numbers of (0,1).

Manuscript received Oct. 10, 2013, revision received Nov. 12, 2013, and final revision received Jan. 28, 2014.